Geophysical Research Letters

RESEARCH LETTER
10.1029/2023GL107737

Offline Correction of CMIP6 HighResMIP Simulated Surface Solar Irradiance With 3D Sub-Grid Terrain Radiative Effects

Chunlei Gu[1], Anning Huang[1,2], Xin Li[3], and Yang Wu[3]

[1]School of Atmospheric Sciences, Nanjing University, Nanjing, China, [2]Qinghai Lake Comprehensive Observation Research Station, Chinese Academy of Sciences, Gangcha, China, [3]Key Laboratory of Transportation Meteorology of China Meteorological Administration, Nanjing Joint Institute for Atmospheric Sciences, Chinese Academy of Meteorological Sciences—Jiangsu Meteorological Service, Nanjing, China

Key Points:

- The biases of surface solar irradiance (SSI) simulated by the CMIP6 HighResMIP models increase with the sub-grid terrain complexity
- The biases of simulated SSI over rugged areas can be clearly reduced by the 3DSTSRE offline correction
- The 3DSTSRE should be considered in the climate models to improve the SSI simulation over rugged areas

Supporting Information:

Supporting Information may be found in the online version of this article.

Correspondence to:

A. Huang,
anhuang@nju.edu.cn

Citation:

Gu, C., Huang, A., Li, X., & Wu, Y. (2024). Offline correction of CMIP6 HighResMIP simulated surface solar irradiance with 3D sub-grid terrain radiative effects. *Geophysical Research Letters*, *51*, e2023GL107737. https://doi.org/10.1029/2023GL107737

Received 7 DEC 2023
Accepted 10 APR 2024

Author Contributions:

Conceptualization: Chunlei Gu, Anning Huang, Xin Li
Data curation: Chunlei Gu, Yang Wu
Formal analysis: Chunlei Gu
Investigation: Chunlei Gu
Methodology: Chunlei Gu, Anning Huang, Xin Li
Resources: Chunlei Gu, Yang Wu
Software: Chunlei Gu, Anning Huang
Supervision: Anning Huang
Validation: Chunlei Gu, Anning Huang
Visualization: Chunlei Gu
Writing – original draft: Chunlei Gu, Anning Huang, Xin Li
Writing – review & editing: Chunlei Gu, Anning Huang, Xin Li, Yang Wu

© 2024. The Author(s).
This is an open access article under the terms of the Creative Commons Attribution License, which permits use, distribution and reproduction in any medium, provided the original work is properly cited.

Abstract The surface solar irradiance (SSI) is crucial for the land-atmosphere processes and remarkably affected by the topography over the rugged areas. However, the Coupled Model Intercomparison Project Phase 6 (CMIP6) HighResMIP models adopting the parallel-plane radiative scheme without considering the sub-grid terrain solar radiative effects (3DSTSRE) overestimate the SSI in the rugged areas and the overestimation increases with the sub-grid terrain complexity. To reduce the biases of the SSI simulations, this study offline corrects the SSI simulations of CMIP6 HighResMIP models by a 3DSTSRE scheme. Results show that the SSI biases produced by the HighResMIP models in the rugged regions can be significantly reduced by adopting the 3DSTSRE offline correction, and the improvements increase with the sub-grid terrain complexity, indicating that considering the 3DSTSRE in the climate models to improve the SSI simulations over rugged areas is necessary.

Plain Language Summary The surface incident solar radiation greatly affected by terrains plays important roles in various processes between the land and atmosphere. However, the Coupled Model Intercomparison Project Phase 6 (CMIP6) HighResMIP models without considering the 3D sub-grid terrain solar radiative effect (3DSTSRE) largely overestimate the surface incident solar radiation over the rugged areas. In this study, adopting a 3DSTSRE scheme to offline correct the surface incident solar radiation simulations from the CMIP6 HighResMIP models can clearly reduce the biases over the rugged areas, and the improvements increase with the sub-grid terrain complexity, implying that the 3DSTSRE should be considered in the climate models to improve the surface incident solar radiation simulation over the rugged areas.

1. Introduction

Surface solar irradiance (SSI) is decisive to the surface energy balance, crucial for the land-atmosphere processes, and the ultimate energy driving the atmospheric motion (Liang et al., 2019; Wild, 2017). The SSI is regulated by the atmospheric and land surface conditions, such as the cloud, aerosol, gas molecule, and topography (Chakraborty & Lee, 2021; Firozjaei et al., 2020; Yang et al., 2016). The solar radiative effects of the atmospheric molecule, cloud, and aerosol are relatively homogenous over the region with tens of kilometers in diameter (Matus & L'Ecuyer, 2017; Yu et al., 2021). However, the terrains considerably increase the heterogenization in the spatial-temporal distribution of the SSI at the local scale (Nunez, 1980; Olson et al., 2019; Proy et al., 1989). The SSI fluxes over the rugged areas are reduced by the shading effects of local and surrounding terrains and added by the reflected solar radiation from the adjacent terrain (Chu et al., 2021; Dozier & Frew, 1990; Hay, 1993; Li et al., 2002). The solar radiation reflected from the surrounding snow-covered terrain can exceed 180 $W{\cdot}m^{-2}$ and account 60% of the total SSI at the typical mid-latitude alpine valley (von Rütte et al., 2021). The late sunrise and early sunset generally occur in the valleys with the different configurations of the terrains, which shorten the daily sunshine duration by several minutes to hours (Adamu et al., 2019; Chen, 2020; Zhang et al., 2018). The shading and obstruction of the sky by the terrains also decreases the SSI value by the average magnitude of 10^1 $W{\cdot}m^{-2}$ and maximum magnitude of 10^2 $W{\cdot}m^{-2}$ (Hao et al., 2019; Wang et al., 2018; Yan et al., 2018). For example, the daily SSI over the lower part of the Arizona's Meteor Crater is 6% lower than that over the crater rim and the maximum decrease of instantaneous SSI is ~300 $W{\cdot}m^{-2}$ (Hoch & Whiteman, 2015).

Due to the essential roles of the SSI in the earth system, to accurately describe the processes determining the SSI in the numerical models has long been an important task (Edwards, 2011; Giorgi et al., 1993). Previous efforts focused on improving the description of radiative forcing by the cloud, aerosol, and atmospheric molecules (Randles et al., 2013; Ritter & Geleyn, 1992; Yi et al., 2016; Zakey et al., 2006). With the continuous increase of model resolution, the sub-grid scale terrain solar radiative effects (STSRE) become significant and nonnegligible in the numerical models (Colette et al., 2003; Essery & Marks, 2007; Hauge & Hole, 2003; Ruiz-Arias et al., 2011). During the last two decades, numerous studies have attempted to consider the STSRE in the numerical models (Liou et al., 2007; Manners et al., 2012; Müller & Scherer, 2005; Zhang et al., 2006, 2022).

Three kinds of STSRE schemes have been developed based on the 2-dimensional idealized terrain radiation theory, the 3-dimensional real terrain radiation theory, and the Monte Carlo photon tracking technology (Gu et al., 2020; He et al., 2019; Huang et al., 2022; Lai et al., 2010; Lee et al., 2011). Numerical studies show that those schemes decline the biases of simulated SSI by 10–100 of watts per square meter for the normal and extreme case over the rugged areas respectively, and the improvement of the simulated SSI increases along with the increase of the horizontal resolution and sub-grid terrain complexity (Arthur et al., 2018; Cai et al., 2023; Fan et al., 2019; Gu et al., 2012; Lee et al., 2013, 2019). The improved simulation of SSI leads to the better performance of the numerical models in reproducing the surface energy balance and thereafter temperature, atmospheric circulation, precipitation, etcetera (Feng & Zhang, 2007; Gu et al., 2022; Hao et al., 2021). However, these attempts are mostly conducted in the regional weather/climate models or land surface models instead of the global climate models (GCM). Although the uncertainty of the SSI simulated by the GCMs over the rugged areas have not been clearly revealed due to the lack of in situ observation in the previous studies (Hu et al., 2019; Markovic et al., 2008; Niu et al., 2023; Wang et al., 2022; Wild, 2008; Xu et al., 2022), the GCMs with the parallel-plane radiative transfer scheme may share the problems in simulating the SSI over the rugged areas to the regional numerical models due to the absence of the STSRE.

The High Resolution Model Intercomparison Project (HighResMIP, Haarsma et al., 2016) for the World Climate Research Program Coupled Model Intercomparison Project Phase 6 (CMIP6) gathers the state-of-the-art GCMs. The CMIP6 SSI data can provide the forcing data for land surface models or hydrological models and have been widely applied in studies related to potential evapotranspiration, solar energy projection, grain yield projection, and so on (Dutta et al., 2022; He et al., 2022; Heavens, 2021; Kim et al., 2023; Liu et al., 2020; Zheng et al., 2018). The 3D sub-grid terrain solar radiative effects (3DSTSRE) are not considered in the CMIP6 HighResMIP models (Table 1). Since complex terrain covers ∼30% of the world's total land area, it is necessary to evaluate and correct the CMIP6 HighResMIP SSI over the rugged areas. In this study, we preliminarily use the 3DSTSRE scheme (Huang et al., 2022) to offline correct the SSI simulated by the CMIP6 HighResMIP models and investigate to what extent the offline correction of 3DSTSRE can reduce the uncertainty of the simulated SSI over the rugged areas. This study not only provides a method to correct the CMIP6 HighResMIP SSI for SSI-related studies over the areas with complex terrains but also lays a foundation for future studies on online simulations using the GCMs with the 3DSTSRE scheme. The rest of the paper is arranged as follows: Section 2 introduces the data, 3DSTSRE scheme, methodology, and metrics. Section 3 presents the results. Section 4 draws the conclusion and discusses the limitation of this study and planning of future work.

2. Data, Methodology and Metrics

2.1. Data

The data used in this study are listed as follows:

1. The Shuttle Radar Topography Mission (SRTM) Version 4.1 digital elevation model (DEM) data with a horizontal resolution of 3″ (∼90 m), which provide the sub-grid topography in this study.
2. The daily shortwave broadband albedo with a horizontal resolution of 0.05° from the Moderate Resolution Imaging Spectroradiometer (Moderate Resolution Imaging Spectroradiometer (MODIS)) MCD43C3 Version 6.1 during 2001–2014 (Schaaf & Wang, 2021).
3. The SSI fluxes during 2001–2014 from the 11 models participating the hist-1950 experiment of the CMIP6 HighResMIP (details in Table 1). Four models (BCC-CSM2-HR, EC-Earth3P-HR, FGOALS-f3-H, and HadGEM3-GC31-HH) provide the 3 hourly SSI while the other seven models (CESM1-CAM5-SE-HR, CMCC-CM2-VHR4, CNRM-CM6-1-HR, ECMWF-IFS-HR, GFDL-CM4C192, INM-CM5-H, and MPI-ESM1-2-XR) only provide the monthly SSI.

Geophysical Research Letters

10.1029/2023GL107737

Table 1
The Models of Coupled Model Intercomparison Project Phase 6 HighResMIP Providing the Data in This Study

Model	Abbreviation	Horizontal resolution	Institution	Model description	Data source
BCC-CSM2-HR*	BCC	~50 km	Beijing Climate Center	Wu et al. (2021)	Jie et al. (2020)
CESM1-CAM5-SE-HR	CESM1	~25 km	National Center for Atmospheric Research, Climate and Global Dynamics Laboratory	Chang et al. (2020)	Hurrel et al. (2020)
CMCC-CM2-VHR4	CMCC	~25 km	Fondazione Centro Euro-Mediterraneo sui Cambiamenti Climatici	Scoccimarro et al. (2022)	Scoccimarro et al. (2018)
CNRM-CM6-1-HR	CNRM	~50 km	Center National de Recherches Meteorologiques, Center Europeen de Recherche et de Formation Avancee en Calcul Scientifique	Saint-Martin et al. (2021)	Voldoire (2019)
EC-Earth3P-HR*	EC-Earth3P	~50 km	EC-Earth-Consortium	Haarsma et al., 2020	EC-Earth Consortium (2018)
ECMWF-IFS-HR	ECWMF	~25 km	European Center for Medium-Range Weather Forecasts	C. Roberts et al. (2018)	C. Roberts et al. (2017)
FGOALS-f3-H*	FGOALS	~25 km	Chinese Academy of Sciences	An et al. (2022)	Y. Yu, (2020)
GFDL-CM4C192	GFDL	~50 km	National Oceanic and Atmospheric Administration, Geophysical Fluid Dynamics Laboratory	Zhao, Golaz et al. (2018)	Zhao, Blanton et al. (2018)
HadGEM3-GC31-HH*	HadGEM3	~50 km	Met Office Hadley Center	M. Roberts et al. (2019)	M. M. Roberts, (2021)
INM-CM5-H	INM	~50 km	Institute for Numerical Mathematics, Russian Academy of Science	Volodin et al. (2017)	Volodin et al. (2019)
MPI-ESM1-2-XR	MPI	~50 km	Max Planck Institute for Meteorology	Gutjahr et al. (2019)	von Storch et al. (2018)

Note. The models with the star (*) provide both the monthly and 3-hourly surface solar irradiance (SSI) data while the other models only provide the monthly SSI data.

4. SSI observations from the monthly CMSAF Cloud, Albedo and Surface Radiation data set (CLARA-A2, Karlsson et al., 2017) with a horizontal resolution of 0.25°, the daily Global LAnd Surface Satellite (GLASS) data set (Liang et al., 2013) with a horizontal resolution of ∼5 km, and the TerraClimate data set of monthly climate and climatic water balance (Abatzoglou et al., 2018) with a horizontal resolution of ∼4 km during 2001–2014. The production of CLARA-A2 SSI considers the terrain effects (Karlsson et al., 2013, 2017). The GLASS and TerraClimate data sets include the satellite observations with the high horizontal resolution of 500–1,000 m as source data, which present the SSI over the complex terrain to a certain extent.

2.2. 3DSTSRE Scheme

As shown in Figure 1a, the SSI over the rugged areas ($E_{t\downarrow}$) is greatly impacted by the local and surrounding terrains. $E_{t\downarrow}$ includes three components, namely, the direct solar radiation ($E_{\mathrm{dirt}\downarrow}$), diffuse solar radiation ($E_{\mathrm{difft}\downarrow}$), and additional solar radiation reflected from the surrounding terrain ($E_{\mathrm{reft}\downarrow}$) (Dozier & Frew, 1990). The $E_{\mathrm{dirt}\downarrow}$ is influenced by the shadows cast by the surrounding topography and the slope and slope orientation of the local terrain (self-shielding). The $E_{\mathrm{difft}\downarrow}$ is controlled by the fraction of visible sky in the entire sky which is indicated by the sky view factor (SVF) (Figure 1a, Dirksen et al., 2019). SVF is 1.0 for the plane surface and gradually decreases with the proportions of sky blocked by terrain increasing (Dozier & Frew, 1990). Lower SVF indicates more complex terrain and less SSI due to the obstruction of topography (Jiao et al., 2019). $E_{\mathrm{reft}\downarrow}$ is determined by the surface albedo and the configuration of surrounding terrain.

Figure 1b shows that the sub-grid scale terrains with the horizontal resolution of 3″ fluctuate sharply within a model grid with the horizontal resolution of 0.5°. The sub-grid terrain can significantly affect the grid-scale SSI. However, the GCMs adopt the plane-parallel radiative transfer scheme which treats the sub-grid topography as plane surface and totally ignores the 3DSTSRE. As a model grid with a horizontal resolution of 0.5° contains ∼360,000 sub-grids with the horizontal resolution of 3″, to explicitly calculate the SSI considering the 3DSTSRE at the sub-grids would result in heavy computing burden. Therefore, Huang et al. (2022) developed a 3DSTSRE scheme to correct the SSI components calculated by the plane-parallel radiative transfer scheme based on the static grid-scale terrain correction factors derived from the SRTM DEM data with the horizontal resolution of 3″ and the grid-scale albedo derived from the MODIS data. Detailed introduction for the Huang 3DSTSRE scheme can be found in Text S1 and Figure S1 in Supporting Information S1.

2.3. Offline Correction

As shown in Figure 1c, the 3-hourly SSI simulations of the 4 HighResMIP models (BCC-CSM2-HR, EC-Earth3P-HR, FGOALS-f3-H, and HadGEM3-GC31-HH) are processed to monthly data. Then the monthly SSI simulations of the 11 HighResMIP models are remapped onto the Gaussian grids with a horizontal resolution of 0.5° (here after omitted as "Gaussian grids") using the first-order conservative remapping method (Jones, 1999). The monthly multi-model ensemble (MME) mean SSI simulations of the 11 and 4 HighResMIP models with the plane-parallel radiative transfer scheme are referred as the 11MME_PP and 4MME_PP data, respectively. The suffix "PP" stands for the plane-parallel radiative transfer scheme.

The 3-hourly SSI simulations of the 4 HighResMIP models are offline corrected by the 3DSTSRE scheme at their native grid spacing, then time averaged to the monthly data, and lastly remapped to the Gaussian grids of 0.5°. The monthly SSI fluxes derived from the 3DSTSRE offline corrected 3-hourly SSI simulations of the 4 HighResMIP models are referred as the 4MME_TOP data. The suffix "TOP" stands for including the radiative effects of the topography, indicating the data with the offline correction of 3DSTSRE scheme. The grid-scale direct solar radiation ($E_{\mathrm{dir},p\downarrow}$), diffuse solar radiation ($E_{\mathrm{dif},p\downarrow}$), and albedo ($a_p$) at the plane surface are necessary for the offline correction of 3DSTSRE. In this study, the $E_{\mathrm{dir},p\downarrow}$ and $E_{\mathrm{dif},p\downarrow}$ are derived from the 3-hourly SSI simulations of the four models following the method of the Community Land Model Version 5 (details in Text S2 Supporting Information S1). The grid-scale a_p at the native grids of each of the four models is derived from the MODIS albedo.

Seven of the 11 models only provide the monthly SSI (Table 1), however, the Huang 3DSTSRE scheme cannot correct the monthly SSI without diurnal variation. To solve this issue, the ratios between the monthly SSI during 2001–2014 between the 4MME_TOP and 4MME_PP data are used to represent the monthly radiative effects of the sub-grid terrain. The ratio is calculated by:

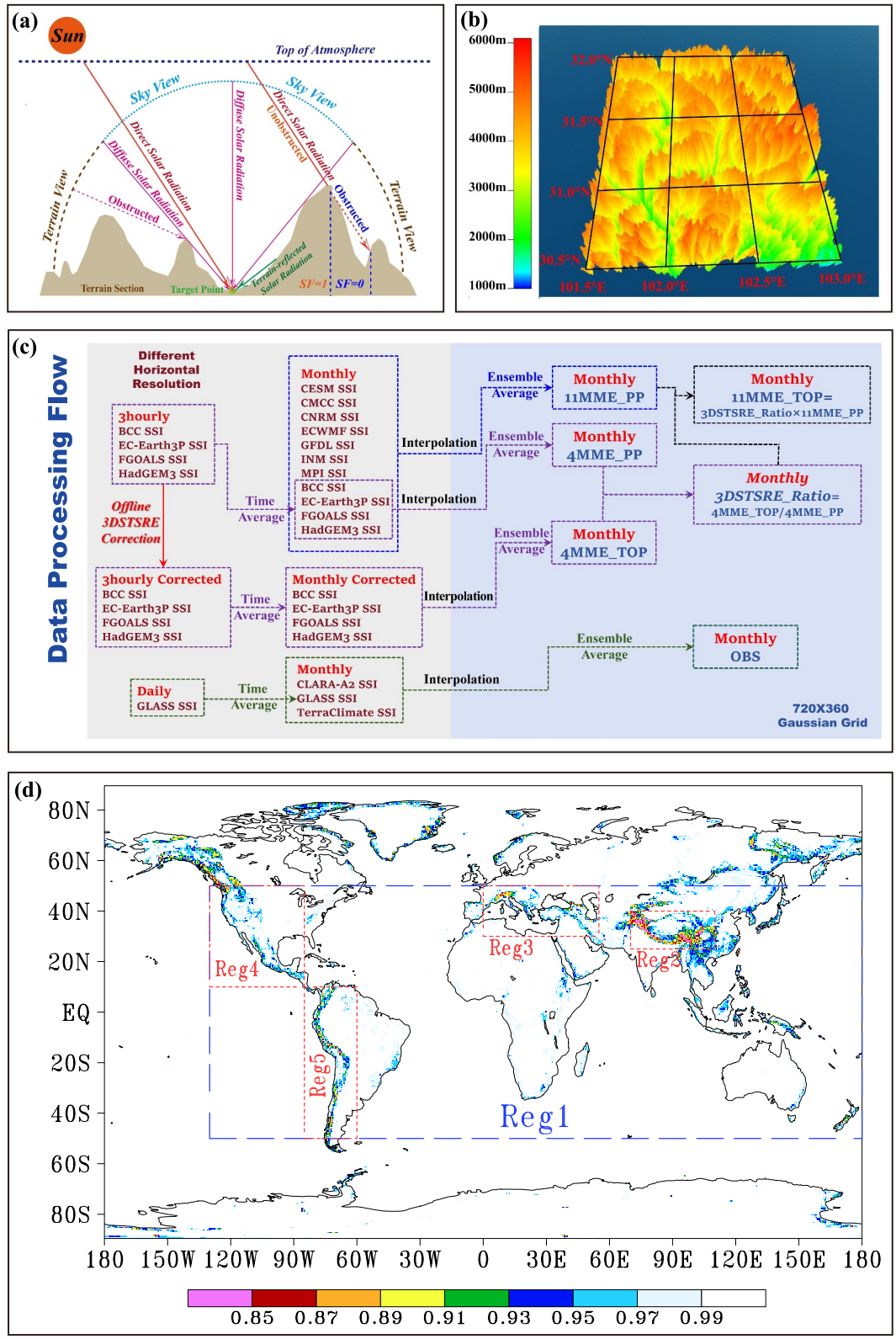

Figure 1. The components of the surface solar irradiance over the rugged terrain (a), the sample diagram of the grid with the horizontal resolution of 0.5° and the sub-grid scale elevation with a horizontal resolution of 3″ in each grid (b), the data processing flow diagram (c), and the grid-scale sky view factor at the Gaussian grids of 0.5° across the world (d). The dashed rectangles in (d) shows the study sub-regions.

$$3\text{DSTSRE\_RATIO} = \frac{\text{SSI}_{4\text{MME\_TOP}}}{\text{SSI}_{4\text{MME\_PP}}} \quad (1)$$

Where the $\text{SSI}_{4\text{MME\_PP}}$ and $\text{SSI}_{4\text{MME\_TOP}}$ are the monthly SSI simulations of the 4MME_PP and 4MME_TOP, respectively. The monthly MME mean SSI simulations of the 11 models offline corrected by the 3DSTSRE (namely the $\text{SSI}_{11\text{MME\_TOP}}$) can be estimated by Equation 2 (see the rationale in Text S3 Supporting Information S1 and Figure S2 Supporting Information S1):

$$\text{SSI}_{11\text{MME\_TOP}} = 3\text{DSTSRE\_RATIO} \cdot \text{SSI}_{11\text{MME\_PP}} \quad (2)$$

where $\text{SSI}_{11\text{MME\_PP}}$ are the monthly SSI simulations of the 11MME_PP using the plane-parallel radiative transfer scheme. The $\text{SSI}_{11\text{MME\_TOP}}$ with the 3DSTSRE is stored in the 11MME_TOP data.

The daily GLASS SSI are firstly processed to monthly data. Then the monthly SSI from the CLARA-A2, GLASS, and TerraClimate data sets are remapped to the Gaussian grids of 0.5°, finally, the averages of the monthly observed SSI from the three products at the Gaussian grids of 0.5° are referred as OBS data.

2.4. Metrics

The smaller grid-scale SVF indicate that the sub-grid terrain obstructs the sky over the grid to a greater extent and lead to much stronger impact on the SSI at the grid (Cai et al., 2023). The SSI over the grids with very flat sub-grid scale topographies (SVF ≥ 0.99) are not discussed because the offline 3DSTSRE correction has extremely small impacts on them. Due to the missing values in the observations over the high-latitude areas, the evaluations are conducted over the land of Reg1 (130°W–180°E, 50°S–50°N) indicated by the blue-dash rectangle of Figure 1d. It is clear that most of the grids with strong 3DSTSRE are located in the study area. In addition, four sub-regions highlighted in the red-dashed rectangles are utilized to reveal how the offline correction of the 3DSTSRE scheme operates in various locations (Reg2: 70°E–110°E, 25°N–40°N; Reg3: 0°–55°E, 30°N–50°N; Reg4: 130°W–85°W, 10°N–50°N; Reg5: 85°W–60°W, 50°S–10°N). The relative root mean square error (RRMSE) and relative error (RE) are used to assess the SSI simulations. Smaller RRMSE and absolute RE indicate better simulation of the SSI in quantity. The RRMSE and RE are calculated by:

$$\text{RRMSE} = \frac{\sqrt{\sum_{i=1}^{n}(S_i - O_i)^2}}{\sum_{i=1}^{n} O_i} \times 100\% \quad (3)$$

$$\text{RE} = \frac{S - O}{O} \times 100\% \quad (4)$$

Where O and S represent the observation and simulation, respectively, n is the sample size.

3. Results

From Figure 2, the CMIP6 HighResMIP models clearly overestimated the SSI fluxes at most of the grids with complex terrain compared to the OBS data, and the overestimation increases with the sub-grid terrain complexity increasing or the grid-scale SVF decreasing (Figures 1d, 2f, and 2g). The spatial distribution and magnitude of the SSI biases in the 11MME_PP data remarkably resemble to those in the 4MME_PP (Figures 2f and 2g). The largest overestimation of the SSI is located over the Tibetan Plateau and the Andes with the value more than 45 $\text{W}\cdot\text{m}^{-2}$. After the offline correction of 3DSTSRE scheme, the SSI fluxes over the rugged areas in the 4MME_TOP and 11MME_TOP data can be decreased by 5–45 $\text{W}\cdot\text{m}^{-2}$ compared to those in the 4MME_PP and 11MME_PP data with much larger decreased values over the grids with much more complex terrains (Figures 1d, 2h, and 2i). The RRMSE of the SSI in the 4MME_TOP and 11MME_TOP data are considerably decreased compared to those in the 4MME_PP and 11MME_PP data, indicating that the offline correction of 3DSTSRE scheme can significantly improve the SSI fluxes simulated by the CMIP6 HighResMIP models (Figures 2j and 2k). From Figures 2a–2e, the SSI of the 4MME_PP, 11MME_PP, 4MME_TOP, 11MME_TOP and OBS data averaged over the grids with the SVF ≤ 0.99 are 209.6, 209.4, 200.9, and 200.7, and 187.8 $\text{W}\cdot\text{m}^{-2}$, respectively. Compared to the 4MME_PP and 11MME_PP data, the RE of the SSI simulations in the 4MME_TOP and

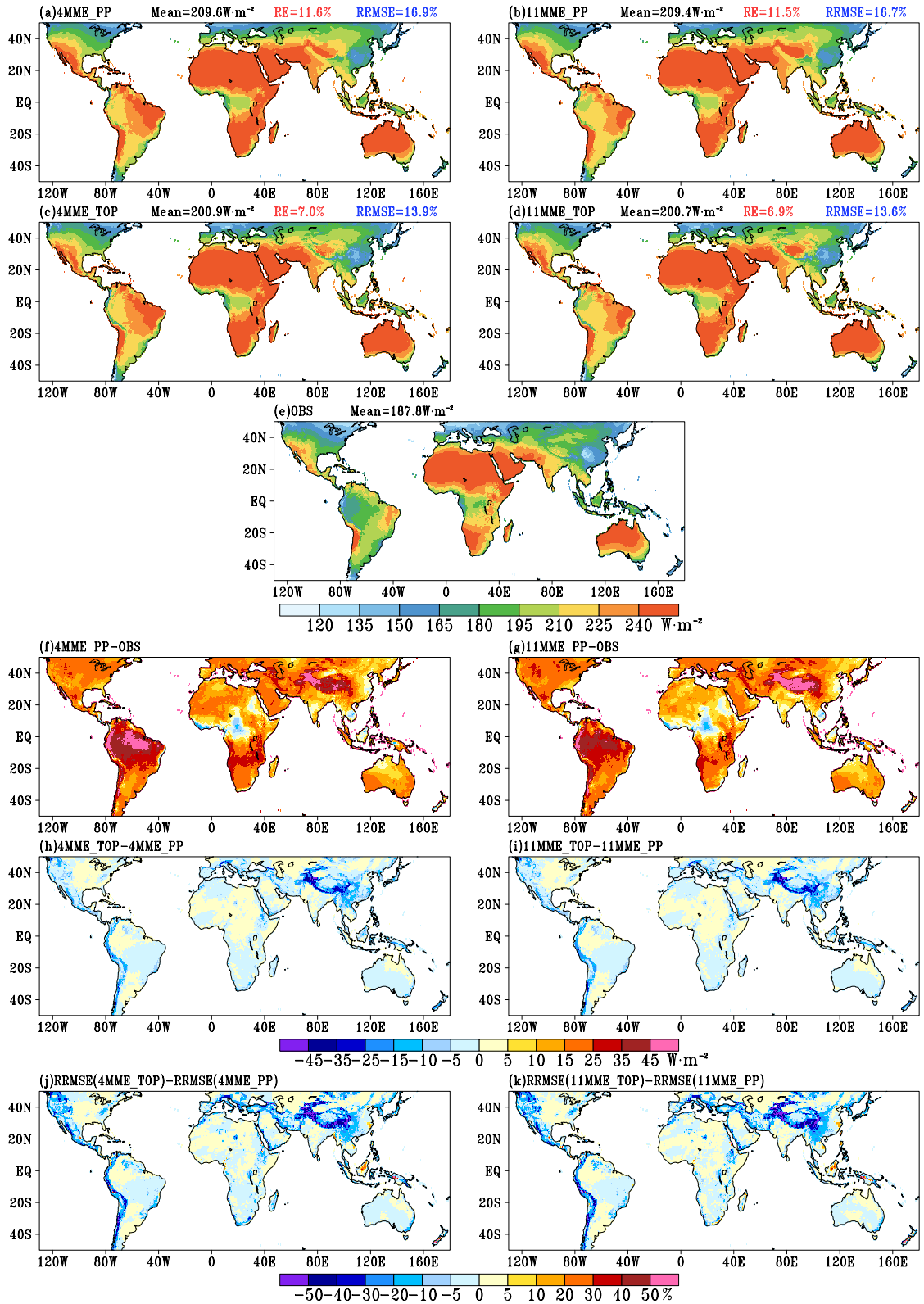
(a)4MME_PP Mean=209.6W·m⁻² RE=11.6% RRMSE=16.9%
(b)11MME_PP Mean=209.4W·m⁻² RE=11.5% RRMSE=16.7%
(c)4MME_TOP Mean=200.9W·m⁻² RE=7.0% RRMSE=13.9%
(d)11MME_TOP Mean=200.7W·m⁻² RE=6.9% RRMSE=13.6%
(e)OBS Mean=187.8W·m⁻²
120 135 150 165 180 195 210 225 240 W·m⁻²
(f)4MME_PP-OBS
(g)11MME_PP-OBS
(h)4MME_TOP-4MME_PP
(i)11MME_TOP-11MME_PP
-45 -35 -25 -15 -10 -5 0 5 10 15 25 35 45 W·m⁻²
(j)RRMSE(4MME_TOP)-RRMSE(4MME_PP)
(k)RRMSE(11MME_TOP)-RRMSE(11MME_PP)
-50 -40 -30 -20 -10 -5 0 5 10 20 30 40 50%
40N 20N EQ 20S 40S
120W 80W 40W 0 40E 80E 120E 160E

Figure 2.

11MME_TOP data at the grids with the SVF ≤ 0.99 can be reduced from 11.6% to 7.0% and from 11.5% to 6.9% with the reductions of 39.7% and 40.0%, respectively, and the RRMSE of the SSI simulations in the 4MME_TOP and 11MME_TOP data at the grids with the SVF ≤ 0.99 are reduced from 16.9% to 13.9% and from 16.7% to 13.6% with the reductions of 17.8% and 18.7%, respectively.

The RRMSE of the SSI simulations in the 4MME_PP and 11MME_PP in each sub-region all increases with the grid-scale SVF decreasing or sub-grid terrain complexity increasing (Figures 3a–3e), indicating the important impact of the 3DSTSRE and the necessity of the terrain correction. Adopting the offline correction of 3DSTSRE scheme can clearly reduce the RRMSE of the SSI simulations in the 4MME_PP and 11MME_PP over each sub-region by 10%–50% with much larger reduction at the grids with much lower SVF (Figures 3f–3j). Meanwhile, the RRMSE of the SSI simulations in the 4MME_TOP and 11MME_TOP including the 3DSTSRE are not sensitive to the sub-grid terrain complexity (Figures 3a–3e), suggesting that the biases in the 4MME_PP and 11MME_PP data due to the absence of the 3DSTSRE can be eliminated by the terrain correction to some extent. However, the RRMSE ranging from 12% to 17% over the sub-regions have been retained in the 4MME_TOP and 11MME_TOP data, which are related to the insufficient description of clouds, aerosols, atmospheric components, etcetera (He et al., 2023; Zheng et al., 2023).

To further illustrate the distribution of the errors in SSI simulations, the probability density function (PDF) and the cumulative density function (CDF) of the absolute relative error (ARE) of the monthly SSI simulations at the grids with the SVF ≤ 0.99 in sub-region Reg1 are illustrated in Figure 4. Compared to the 4MME_PP and 11MME_PP, the PDF of the ARE of the SSI simulations in the 4MME_TOP and 11MME_TOP increases at the AREs less than ∼12% and decreases at the AREs more than ∼12% with the largest increases at the ARE near 0 (Figures 4a and 4b), and the CDF of the ARE of the SSI simulations in the 4MME_TOP and 11MME_TOP is increased by 22.0% and 22.1% at the AREs less than 12% respectively (Figures 4c and 4d), indicating that the offline correction of 3DSTSRE can largely reduce the SSI simulation errors related to the terrain.

Overall, the CMIP6 HighResMIP models overestimate the SSI over the grids with the complex topographies and the overestimation increases with the complexity of the sub-grid terrain. The offline correction of 3DSTSRE scheme can effectively reduce the biases of SSI simulated by the parallel-plane radiative transfer scheme at areas with the complex sub-grid terrains and the improvements increase with the sub-grid terrain complexity.

4. Conclusion and Discussion

The SSI is very important in the land-atmosphere processes and significantly regulated by the topography. However, due to lack of ground-based SSI observations over the rugged areas, the performances of the simulated SSI over the complex terrain by the climate models are not well evaluated. The prosperously developed SSI data, based on observations from high-resolution satellite sensors, provide an invaluable opportunity to study SSI in rugged areas. In addition, the STSRE are still not well concerned in most of numerical models. This study uses the 3DSTSRE scheme to offline correct the simulated SSI fluxes from the CMIP6 HighResMIP Models and take the satellite-derived SSI data containing the information of terrain solar radiative effects as the reference data to evaluate the CMIP6 HighResMIP SSI fluxes over the rugged areas without and with the offline correction of 3DSTSRE scheme.

Without the offline correction of 3DSTSRE, the CMIP6 HighResMIP models obviously overestimate the SSI fluxes over the rugged areas between 50°S and 50°N globally in 2001–2014. The overestimation of the modeled SSI fluxes from each CMIP6 HighResMIP model and from the ensemble of the CMIP6 HighResMIP models increases sharply with the sub-grid scale terrain complexity. The RRMSE of the SSI fluxes from the MME mean of the CMIP6 HighResMIP Models increases from ∼15% to ∼30% with the sub-grid scale terrain complexity increasing.

Figure 2. The surface solar irradiance (SSI) with a horizontal resolution of 0.5° from the 4M_PP data (a), the 11M_PP data (b), the 4MME_TOP data (c), the 11MME_TOP data (d), and the OBS data (e) averaged over 2001–2014. The differences of the 14-year mean SSI fluxes between the 4MME_PP data and the OBS data (f), between the 11MME_PP data and the OBS data (g), between the 4MME_TOP data and the 4MME_PP data (h), and between the 11MME_TOP data and the 11MME_PP data (i). The differences of the relative root mean square errors (RRMSE) of the SSI between the 4MME_TOP data and the 4MME_PP data (j) and between the 11MME_TOP data and the 11MME_PP data (k) during 2001–2014. The black numbers in Figures (a–e) are the SSI averaged at the grids with SVF ≤ 0.99 in the sub-region Reg1 shown in Figure 1d. The red and blue numbers in Figures a–d are the relative errors of the 14-year mean SSI simulations and relative root mean square errors of the SSI simulations during 2001–2014 at the grids with SVF ≤ 0.99 in the sub-region Reg1 shown in Figure 1d, respectively.

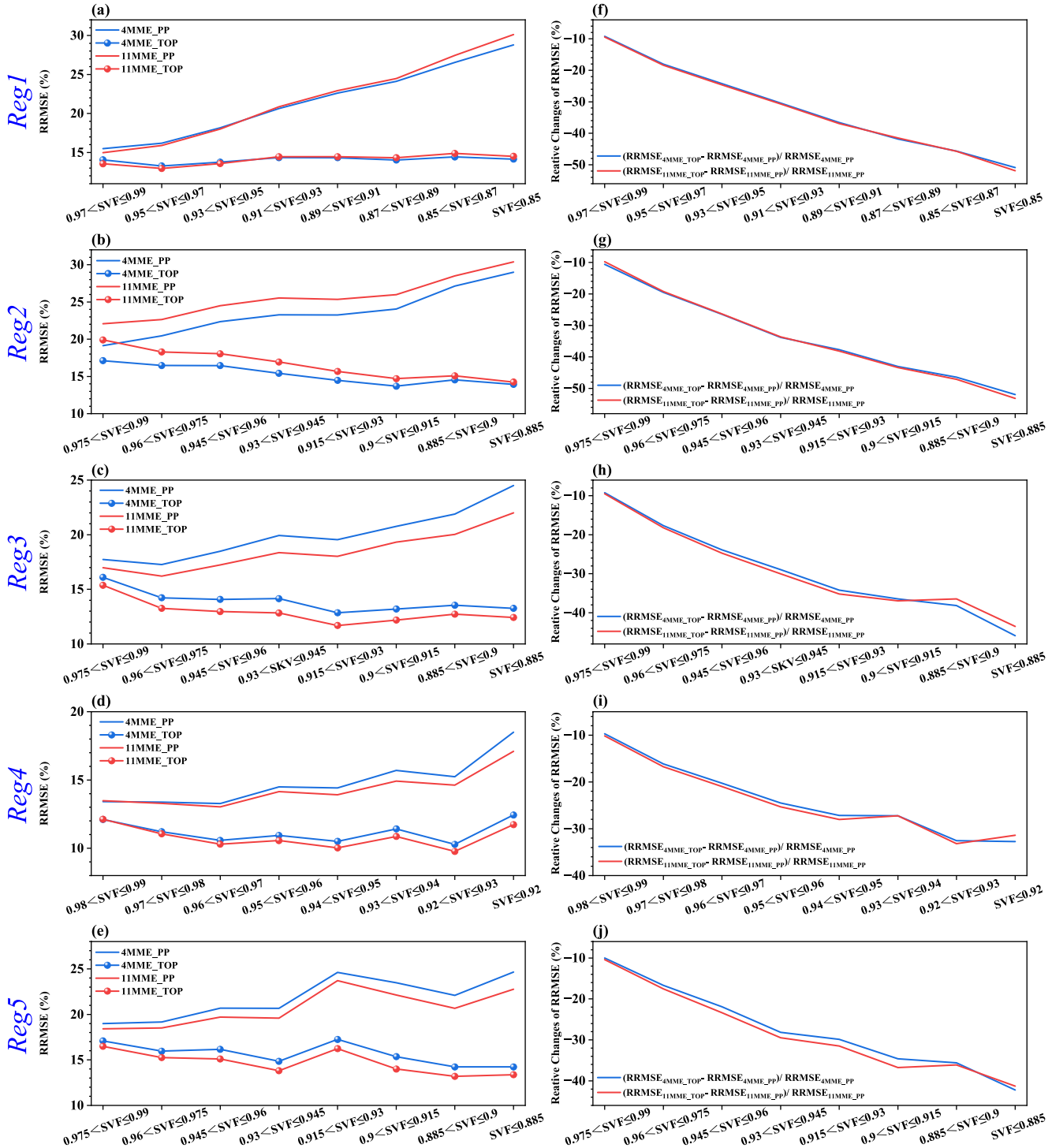

Figure 3. The relative root mean square errors of the surface solar irradiance (SSI) simulations from the 4MME_PP, 11MME_PP, 4MME_TOP, and 11MME_TOP data during 2001–2014 (a–e), and the relative changes of the relative root mean square errors of the SSI simulations with the 3DSTSRE offline correction during 2001–2014 compared to those without the 3DSTSRE offline correction at the grids with different grid-scale SVF in different sub-regions (f–j). Each sub-region is shown in Figure 1d.

The offline correction of the 3DSTSRE scheme can effectively reduce the biases of simulated SSI fluxes from the MME mean of CMIP6 HighResMIP Models. For the grids with the most complex sub-grid terrain, the RRMSE of the SSI simulated by the CMIP6 models can be reduced by ~50% due to the offline correction of 3DSTSRE scheme. Therefore, it is necessary, urgent, and beneficial to describe the 3DSTSRE into the climate modeling.

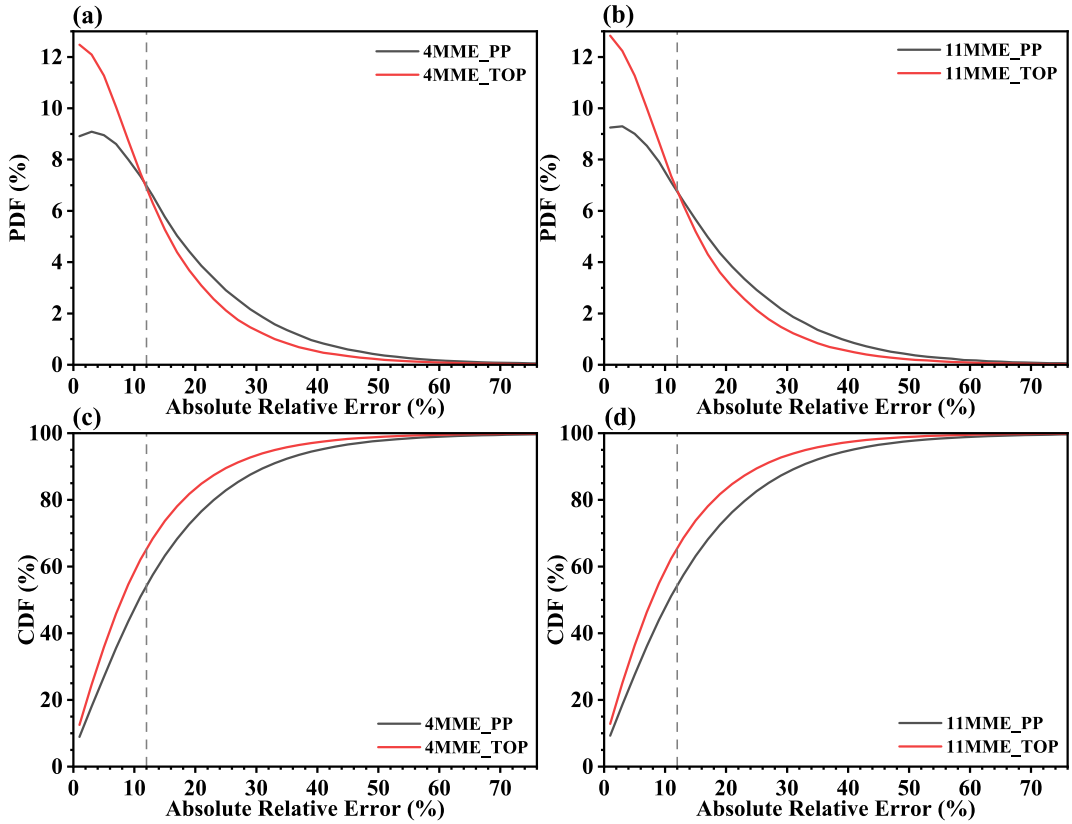

Figure 4. The probability density function (PDF, a, b) and the cumulative density function (CDF, c, d) of the absolute relative error of the monthly surface solar irradiance simulations in the 4MME_PP, 4MME_TOP, 11MME_PP, and 11MME_TOP data at the grids with SVF ≤ 0.99 in the sub-region Reg1 during 2001–2014.

However, we have to admit that this study has two main shortcomings. One is that the normalized standard deviation of three observed monthly SSI is more than 10% over the Himalayas and Andes (Figure S3 in Supporting Information S1), indicating that the CLARA-A2, GLASS, and TerraClimate data sets exhibit discrepancies in the rugged areas. The simulated SSI are further evaluated by taking the CLARA-A2, GLASS, or TerraClimate alone as the reference data (Figures S4–S9 in Supporting Information S1). Figures S4–S9 in Supporting Information S1 also demonstrate that the RRMSE of the simulated SSI increases with the SVF decreasing, and the offline correction of the 3DSTSRE can clearly reduce the biases of the simulated SSI in the rugged areas, thereby enhancing the confidence in the offline correction of 3DSTSRE. The other one is that this study conducts an offline correction instead of applying the 3DSTSRE scheme to a certain numerical model, which neglects the important feedback in the land-atmosphere processes (such as the cloud, soil, albedo, snow cover, etcetera). We have adopted the 3DSTSRE scheme into the BCC-CSM2-HR model recently and the systematical impacts of the 3DSTSRE scheme on the performance of the BCC-CSM2-HR model will be reported in the future. The remained RRMSE of the SSI over the grids with different sub-grid terrain complexity after the offline correction of 3DSTSRE (Figure 3a) are ~14%, which might come from the insufficient description of the other processes such as the clouds and aerosol. In addition, the reasons for the significant uncertainty in the simulated SSI over the regions with relatively flat terrains (such as the Amazon basin and the Changtang Plateau) should be investigated in the future.

Data Availability Statement

Data: The SRTM DEM data are provided by the International Center for Tropical Agriculture (CIAT) at https://developers.google.com/earth-engine/datasets/catalog/CGIAR_SRTM90_V4; The daily GLASS SSI data (Liang et al., 2013) are retrieved from http://glass.umd.edu/Download.html; The monthly CLARA-A2 SSI data (Karlsson et al., 2020); The monthly TerraClimate SSI data (Abatzoglou et al., 2017); The monthly and 3-hourly

SSI data from the hist-1950 experiment of CMIP6 HighResMIP are offered by the Earth System Grid Federation (ESGF) at https://aims2.llnl.gov/search. The specific CMIP6 HighResMIP models used in this study are listed in Table 1; and the daily MODIS MCD43C3 albedo (Schaaf & Wang, 2021). *Software*: The software for the offline correction of 3DSTSRE is provided by Gu et al. (2023).

Acknowledgments
This study is supported by the National Natural Science Foundation of China under Grant 42375157, the National Key R&D Program of China under Grant 2022YFC3080500, the CAS "Light of West China" Program (E129030101), Open Research Fund Program of Plateau Atmosphere and Environment Key Laboratory of Sichuan Province (PAEKL-2023-K01), the Research Funds for the Frontiers Science Center for Critical Earth Material Cycling Nanjing University, the Fundamental Research Funds for the Central Universities (020914380103), the Jiangsu University "Blue Project" outstanding young teachers training object, the Jiangsu Collaborative Innovation Center for Climate Change, and the Postgraduate Research and Practice Innovation Program of Jiangsu Province (No. 124 in 2023). We appreciate the High Performance Computing Center of Nanjing University and the National Key Scientific and Technological Infrastructure project "Earth System Numerical Simulation Facility" (EarthLab) for providing us the computing resource. We are grateful to ESGF, NASA, CIAT, UMD, EUMETSAT, and Abatzoglou et al. (2018) for allowing us to use their data sets. We show our warm appreciation and deepest respect to the editor and two anonymous reviewers for their constructive suggestions to greatly improve the manuscript.

References

Abatzoglou, J. T., Dobrowski, S. Z., Parks, S. A., & Hegewisch, K. C. (2017). Monthly climate and climatic water balance for global terrestrial surfaces from 1958–2015 [Dataset]. *University of Idaho Applied Climate Science Lab*. https://doi.org/10.7923/G43J3B0R

Abatzoglou, J. T., Dobrowski, S. Z., Parks, S. A., & Hegewisch, K. C. (2018). TerraClimate, a high-resolution global dataset of monthly climate and climatic water balance from 1958–2015. *Scientific Data*, *5*(1), 170191. https://doi.org/10.1038/sdata.2017.191

Adamu, M., Qiu, X., Shi, G., Nooni, I. K., Wang, D., Zhu, X., et al. (2019). High spatial resolution simulation of sunshine duration over the complex terrain of Ghana. *Sensors*, *19*(7), 1743. https://doi.org/10.3390/s19071743

An, B., Yu, Y., Bao, Q., He, B., Li, J., Luan, Y., et al. (2022). CAS FGOALS-f3-H dataset for the High-Resolution Model Intercomparison Project (HighResMIP) tier 2. *Advances in Atmospheric Sciences*, *39*(11), 1873–1884. https://doi.org/10.1007/s00376-022-2030-5

Arthur, R. S., Lundquist, K. A., Mirocha, J. D., & Chow, F. K. (2018). Topographic effects on radiation in the WRF model with the immersed boundary method: Implementation, validation, and application to complex terrain. *Monthly Weather Review*, *146*(10), 3277–3292. https://doi.org/10.1175/mwr-d-18-0108.1

Cai, S., Huang, A., Zhu, K., Guo, W., Wu, Y., & Gu, C. (2023). The forecast skill of the summer precipitation over Tibetan plateau improved by the adoption of a 3D sub-grid terrain solar radiative effect scheme in a convection-permitting model. *Journal of Geophysical Research: Atmospheres*, *128*(11), e2022JD038105. https://doi.org/10.1029/2022JD038105

Chakraborty, T., & Lee, X. (2021). Large differences in diffuse solar radiation among current-generation reanalysis and satellite-derived products. *Journal of Climate*, *34*(16), 6635–6650. https://doi.org/10.1175/JCLI-D-20-0979.1

Chang, P., Zhang, S., Danabasoglu, G., Yeager, S. G., Fu, H., Wang, H., et al. (2020). An unprecedented set of high-resolution Earth system simulations for understanding multiscale interactions in climate variability and change. *Journal of Advances in Modeling Earth Systems*, *12*(12), e2020MS002298. https://doi.org/10.1029/2020MS002298

Chen, N. (2020). Deriving the slope-mean shielded astronomical solar radiation spectrum and slope-mean possible sunshine duration spectrum over the Loess Plateau. *Journal of Mountain Science*, *17*(1), 133–146. https://doi.org/10.1007/s11629-018-5246-1

Chu, Q., Yan, G., Qi, J., Mu, X., Li, L., Tong, Y., et al. (2021). Quantitative analysis of terrain reflected solar radiation in snow-covered mountains: A case study in Southeastern Tibetan plateau. *Journal of Geophysical Research: Atmospheres*, *126*(11), e2020JD034294. https://doi.org/10.1029/2020JD034294

Colette, A., Chow, F. K., & Street, R. L. (2003). A numerical study of inversion-layer breakup and the effects of topographic shading in idealized valleys. *Journal of Applied Meteorology*, *42*(9), 1255–1272. https://doi.org/10.1175/1520-0450(2003)042<1255:Ansoib>2.0.Co;2

Dirksen, M., Ronda, R. J., Theeuwes, N. E., & Pagani, G. A. (2019). Sky view factor calculations and its application in urban heat island studies. *Urban Climate*, *30*, 100498. https://doi.org/10.1016/j.uclim.2019.100498

Dozier, J., & Frew, J. (1990). Rapid calculation of terrain parameters for radiation modeling from digital elevation data. *IEEE Transactions on Geoscience and Remote Sensing*, *28*(5), 963–969. https://doi.org/10.1109/36.58986

Dutta, R., Chanda, K., & Maity, R. (2022). Future of solar energy potential in a changing climate across the world: A CMIP6 multi-model ensemble analysis. *Renewable Energy*, *188*, 819–829. https://doi.org/10.1016/j.renene.2022.02.023

EC-Earth Consortium. (2018). EC-Earth-Consortium EC-Earth3P-HR model output prepared for CMIP6 HighResMIP hist-1950 [Dataset]. *Earth System Grid Federation*. https://doi.org/10.22033/ESGF/CMIP6.4683

Edwards, P. N. (2011). History of climate modeling. *WIREs Climate Change*, *2*(1), 128–139. https://doi.org/10.1002/wcc.95

Essery, R., & Marks, D. (2007). Scaling and parametrization of clear-sky solar radiation over complex topography. *Journal of Geophysical Research*, *112*(D10), D10122. https://doi.org/10.1029/2006jd007650

Fan, X., Gu, Y., Liou, K.-N., Lee, W.-L., Zhao, B., Chen, H., & Lu, D. (2019). Modeling study of the impact of complex terrain on the surface energy and hydrology over the Tibetan Plateau. *Climate Dynamics*, *53*(11), 6919–6932. https://doi.org/10.1007/s00382-019-04966-z

Feng, L., & Zhang, Y. (2007). Impacts of the thermal effects of sub-grid orography on the heavy rainfall events along the Yangtze River Valley in 1991. *Advances in Atmospheric Sciences*, *24*(5), 881–892. https://doi.org/10.1007/s00376-007-0881-4

Firozjaei, H. K., Firozjaei, M. K., Nematollahi, O., Kiavarz, M., & Alavipanah, S. K. (2020). On the effect of geographical, topographic and climatic conditions on feed-in tariff optimization for solar photovoltaic electricity generation: A case study in Iran. *Renewable Energy*, *153*, 430–439. https://doi.org/10.1016/j.renene.2020.01.127

Giorgi, F., Marinucci, M. R., & Bates, G. T. (1993). Development of a second-generation Regional Climate Model (RegCM2). Part I: Boundary-layer and radiative transfer processes. *Monthly Weather Review*, *121*(10), 2794–2813. https://doi.org/10.1175/1520-0493(1993)121<2794:DOASGR>2.0.CO;2

Gu, C., Huang, A., Li, X., & Wu, Y. (2023). Source codes for offline correction of CMIP6 HighResMIP simulated surface solar irradiance with 3D sub-grid terrain radiative effects [Software]. *Zenodo*. https://doi.org/10.5281/zenodo.10700690

Gu, C., Huang, A., Wu, Y., Yang, B., Mu, X., Zhang, X., & Cai, S. (2020). Effects of subgrid terrain radiative forcing on the ability of RegCM4.1 in the simulation of summer precipitation over China. *Journal of Geophysical Research: Atmospheres*, *125*(12), e2019JD032215. https://doi.org/10.1029/2019jd032215

Gu, C., Huang, A., Zhang, Y., Yang, B., Cai, S., Xu, X., et al. (2022). The wet bias of RegCM4 over Tibet plateau in summer reduced by adopting the 3D sub-grid terrain solar radiative effect parameterization scheme. *Journal of Geophysical Research: Atmospheres*, *127*(21), e2022JD037434. https://doi.org/10.1029/2022JD037434

Gu, Y., Liou, K. N., Lee, W. L., & Leung, L. R. (2012). Simulating 3-D radiative transfer effects over the Sierra Nevada Mountains using WRF. *Atmospheric Chemistry and Physics*, *12*(20), 9965–9976. https://doi.org/10.5194/acp-12-9965-2012

Gutjahr, O., Putrasahan, D., Lohmann, K., Jungclaus, J. H., von Storch, J. S., Brüggemann, N., et al. (2019). Max Planck Institute Earth System Model (MPI-ESM1.2) for the High-Resolution Model Intercomparison Project (HighResMIP). *Geoscientific Model Development*, *12*(7), 3241–3281. https://doi.org/10.5194/gmd-12-3241-2019

Haarsma, R., Acosta, M., Bakhshi, R., Bretonnière, P. A., Caron, L. P., Castrillo, M., et al. (2020). HighResMIP versions of EC-Earth: EC-Earth3P and EC-Earth3P-HR – Description, model computational performance and basic validation. *Geoscientific Model Development*, *13*(8), 3507–3527. https://doi.org/10.5194/gmd-13-3507-2020

Haarsma, R. J., Roberts, M. J., Vidale, P. L., Senior, C. A., Bellucci, A., Bao, Q., et al. (2016). High Resolution Model Intercomparison Project (HighResMIP v1.0) for CMIP6. *Geoscientific Model Development*, *9*(11), 4185–4208. https://doi.org/10.5194/gmd-9-4185-2016

Hao, D., Bisht, G., Gu, Y., Lee, W.-L., Liou, K.-N., & Leung, L. R. (2021). A parameterization of sub-grid topographical effects on solar radiation in the E3SM land model (version 1.0): Implementation and evaluation over the Tibetan plateau. *Geoscientific Model Development*, *14*(10), 1–23. https://doi.org/10.5194/gmd-2021-55

Hao, D., Wen, J., Xiao, Q., Wu, S., Lin, X., You, D., & Tang, Y. (2019). Impacts of DEM geolocation bias on downward surface shortwave radiation estimation over clear-sky rugged terrain: A case study in Dayekou Basin, China. *IEEE Geoscience and Remote Sensing Letters*, *16*(1), 10–14. https://doi.org/10.1109/LGRS.2018.2868563

Hauge, G., & Hole, L. R. (2003). Implementation of slope irradiance in Mesoscale Model version 5 and its effect on temperature and wind fields during the breakup of a temperature inversion. *Journal of Geophysical Research*, *108*(D2), 4058. https://doi.org/10.1029/2002jd002575

Hay, J. E. (1993). Calculating solar radiation for inclined surfaces: Practical approaches. *Renewable Energy*, *3*(4), 373–380. https://doi.org/10.1016/0960-1481(93)90104-O

He, J., Hong, L., Shao, C., & Tang, W. (2023). Global evaluation of simulated surface shortwave radiation in CMIP6 models. *Atmospheric Research*, *292*, 106896. https://doi.org/10.1016/j.atmosres.2023.106896

He, S., Smirnova, T. G., & Benjamin, S. G. (2019). A scale-Aware parameterization for estimating subgrid variability of downward solar radiation using high-resolution digital elevation model data. *Journal of Geophysical Research: Atmospheres*, *124*(24), 13680–13692. https://doi.org/10.1029/2019jd031563

He, Y., Yang, K., Wild, M., Wang, K., Tong, D., Shao, C., & Zhou, T. (2022). Constrained future brightening of solar radiation and its implication for China's solar power. *National Science Review*, *10*(1), nwac242. https://doi.org/10.1093/nsr/nwac242

Heavens, N. G. (2021). Downscaling CESM2 in CLM5 to hindcast preindustrial equilibrium line altitudes for tropical mountain glaciers. *Geophysical Research Letters*, *48*(17), e2021GL094071. https://doi.org/10.1029/2021GL094071

Hoch, S. W., & Whiteman, C. D. (2015). Topographic effects on the surface radiation balance in and around Arizona's Meteor Crater. *Journal of Applied Meteorology and Climatology*, *49*(6), 1114–1128. https://doi.org/10.1175/2010JAMC2353.1

Huang, A., Gu, C., Zhang, Y., Li, W., Zhang, L., Wu, Y., et al. (2022). Development of a clear-sky 3D sub-grid terrain solar radiative effect parameterization scheme based on the mountain radiation theory. *Journal of Geophysical Research: Atmospheres*, *127*(13), e2022JD036449. https://doi.org/10.1029/2022jd036449

Hu, G., Zhao, L., Li, R., Wu, X., Wu, T., Zhu, X., et al. (2019). Simulation of land surface heat fluxes in permafrost regions on the Qinghai-Tibetan Plateau using CMIP5 models. *Atmospheric Research*, *220*, 155–168. https://doi.org/10.1016/j.atmosres.2019.01.006

Hurrel, J., Holland, M., Gent, P., Ghan, S., Kay, J., Kushner, P., et al. (2020). NCAR CESM1-CAM5-SE-HR model output prepared for CMIP6 [Dataset]. *HighResMIP hist-1950*. https://doi.org/10.22033/ESGF/CMIP6.14294

Jiao, Z. H., Ren, H., Mu, X., Zhao, J., Wang, T., & Dong, J. (2019). Evaluation of four sky view factor algorithms using digital surface and elevation model data. *Earth and Space Science*, *6*(2), 222–237. https://doi.org/10.1029/2018EA000475

Jie, W., Zhang, J., Wu, T., Shi, X., Zhang, F., Li, J., et al. (2020). BCC BCC-CSM2HR model output prepared for CMIP6 HighResMIP hist-1950 [Dataset]. *Earth System Grid Federation*. https://doi.org/10.22033/ESGF/CMIP6.2921

Jones, P. W. (1999). First- and second-order conservative remapping schemes for grids in spherical coordinates. *Monthly Weather Review*, *127*(9), 2204–2210. https://doi.org/10.1175/1520-0493(1999)127<2204:FASOCR>2.0.CO;2

Karlsson, K. G., Anttila, K., Trentmann, J., Stengel, M., Fokke Meirink, J., Devasthale, A., et al. (2017). CLARA-A2: The second edition of the CM SAF cloud and radiation data record from 34 years of global AVHRR data. *Atmospheric Chemistry and Physics*, *17*(9), 5809–5828. https://doi.org/10.5194/acp-17-5809-2017

Karlsson, K.-G., Anttila, K., Trentmann, J., Stengel, M., Solodovnik, I., Meirink, J., et al. (2020). CLARA-A2.1: CM SAF cLoud, albedo and surface RAdiation data set from AVHRR data—Edition 2.1 [Dataset]. *Satellite Application Facility on Climate Monitoring*. https://doi.org/10.5676/EUM_SAF_CM/CLARA_AVHRR/V002_01

Karlsson, K. G., Riihelä, A., Müller, R., Meirink, J. F., Sedlar, J., Stengel, M., et al. (2013). CLARA-A1: A cloud, Albedo, and radiation dataset from 28 yr of global AVHRR data. *Atmospheric Chemistry and Physics*, *13*(10), 5351–5367. https://doi.org/10.5194/acp-13-5351-2013

Kim, S., Kim, S., & An, K. (2023). An integrated multi-modeling framework to estimate potential rice and energy production under an agrivoltaic system. *Computers and Electronics in Agriculture*, *213*, 108157. https://doi.org/10.1016/j.compag.2023.108157

Lai, Y. J., Chou, M. D., & Lin, P. H. (2010). Parameterization of topographic effect on surface solar radiation. *Journal of Geophysical Research*, *115*(D1), D01104. https://doi.org/10.1029/2009JD012305

Lee, W.-L., Liou, K. N., & Hall, A. (2011). Parameterization of solar fluxes over mountain surfaces for application to climate models. *Journal of Geophysical Research*, *116*(D1), D01101. https://doi.org/10.1029/2010jd014722

Lee, W.-L., Liou, K. N., & Wang, C.-C. (2013). Impact of 3-D topography on surface radiation budget over the Tibetan Plateau. *Theoretical and Applied Climatology*, *113*(1), 95–103. https://doi.org/10.1007/s00704-012-0767-y

Lee, W.-L., Liou, K.-N., Wang, C.-C., Gu, Y., Hsu, H.-H., & Li, J.-L. F. (2019). Impact of 3-D radiation-topography interactions on surface temperature and energy budget over the Tibetan plateau in winter. *Journal of Geophysical Research: Atmospheres*, *124*(3), 1537–1549. https://doi.org/10.1029/2018JD029592

Liang, S., Wang, D., He, T., & Yu, Y. (2019). Remote sensing of earth's energy budget: Synthesis and review. *International Journal of Digital Earth*, *12*(7), 737–780. https://doi.org/10.1080/17538947.2019.1597189

Liang, S., Zhao, X., Liu, S., Yuan, W., Cheng, X., Xiao, Z., et al. (2013). A long-term Global LAnd Surface Satellite (GLASS) data-set for environmental studies. *International Journal of Digital Earth*, *6*(sup1), 5–33. https://doi.org/10.1080/17538947.2013.805262

Liou, K. N., Lee, W.-L., & Hall, A. (2007). Radiative transfer in mountains: Application to the Tibetan Plateau. *Geophysical Research Letters*, *34*(23), L23809. https://doi.org/10.1029/2007gl031762

Liu, X., Li, C., Zhao, T., & Han, L. (2020). Future changes of global potential evapotranspiration simulated from CMIP5 to CMIP6 models. *Atmospheric and Oceanic Science Letters*, *13*(6), 568–575. https://doi.org/10.1080/16742834.2020.1824983

Li, X., Koike, T., & Cheng, G. (2002). Retrieval of snow reflectance from Landsat data in rugged terrain. *Annals of Glaciology*, *34*, 31–37. https://doi.org/10.3189/172756402781817635

Manners, J., Vosper, S. B., & Roberts, N. (2012). Radiative transfer over resolved topographic features for high-resolution weather prediction. *Quarterly Journal of the Royal Meteorological Society*, *138*(664), 720–733. https://doi.org/10.1002/qj.956

Markovic, M., Jones, C. G., Vaillancourt, P. A., Paquin, D., Winger, K., & Paquin-Ricard, D. (2008). An evaluation of the surface radiation budget over North America for a suite of regional climate models against surface station observations. *Climate Dynamics*, *31*(7), 779–794. https://doi.org/10.1007/s00382-008-0378-6

Matus, A. V., & L'Ecuyer, T. S. (2017). The role of cloud phase in Earth's radiation budget. *Journal of Geophysical Research: Atmospheres*, *122*(5), 2559–2578. https://doi.org/10.1002/2016JD025951

Müller, M. D., & Scherer, D. (2005). A grid- and subgrid-scale radiation parameterization of topographic effects for mesoscale weather forecast models. *Monthly Weather Review*, *133*(6), 1431–1442. https://doi.org/10.1175/mwr2927.1

Niu, J., Qin, W., Wang, L., Zhang, M., Wu, J., & Zhang, Y. (2023). Climate change impact on photovoltaic power potential in China based on CMIP6 models. *Science of the Total Environment*, *858*, 159776. https://doi.org/10.1016/j.scitotenv.2022.159776

Nunez, M. (1980). The calculation of solar and net radiation in mountainous terrain. *Journal of Biogeography*, *7*(2), 173–186. https://doi.org/10.2307/2844709

Olson, M., Rupper, S., & Shean, D. E. (2019). Terrain induced biases in clear-sky shortwave radiation due to digital elevation model resolution for glaciers in complex terrain. *Frontiers in Earth Science*, *7*, 216. https://doi.org/10.3389/feart.2019.00216

Proy, C., Tanré, D., & Deschamps, P. Y. (1989). Evaluation of topographic effects in remotely sensed data. *Remote Sensing of Environment*, *30*(1), 21–32. https://doi.org/10.1016/0034-4257(89)90044-8

Randles, C. A., Kinne, S., Myhre, G., Schulz, M., Stier, P., Fischer, J., et al. (2013). Intercomparison of shortwave radiative transfer schemes in global aerosol modeling: Results from the AeroCom radiative transfer experiment. *Atmospheric Chemistry and Physics*, *13*(5), 2347–2379. https://doi.org/10.5194/acp-13-2347-2013

Ritter, B., & Geleyn, J.-F. (1992). A comprehensive radiation scheme for numerical weather prediction models with potential applications in climate simulations. *Monthly Weather Review*, *120*(2), 303–325. https://doi.org/10.1175/1520-0493(1992)120<0303:ACRSFN>2.0.CO;2

Roberts, C. D., Senan, R., Molteni, F., Boussetta, S., & Keeley, S. (2017). ECMWF ECMWF-IFS-HR model output prepared for CMIP6 HighResMIP hist-1950 [Dateset]. *Earth System Grid Federation*. https://doi.org/10.22033/ESGF/CMIP6.4981

Roberts, C. D., Senan, R., Molteni, F., Boussetta, S., Mayer, M., & Keeley, S. P. E. (2018). Climate model configurations of the ECMWF Integrated Forecasting System (ECMWF-IFS cycle 43r1) for HighResMIP. *Geoscientific Model Development*, *11*(9), 3681–3712. https://doi.org/10.5194/gmd-11-3681-2018

Roberts, M. (2021). MOHC HadGEM3-GC31-HH model output prepared for CMIP6 HighResMIP hist-1950 [Dataset]. *Earth System Grid Federation*. https://doi.org/10.22033/ESGF/CMIP6.6038

Roberts, M. J., Baker, A., Blockley, E. W., Calvert, D., Coward, A., Hewitt, H. T., et al. (2019). Description of the resolution hierarchy of the global coupled HadGEM3-GC3.1 model as used in CMIP6 HighResMIP experiments. *Geoscientific Model Development*, *12*(12), 4999–5028. https://doi.org/10.5194/gmd-12-4999-2019

Ruiz-Arias, J. A., Pozo-Vázquez, D., Lara-Fanego, V., Santos-Alamillos, F. J., & Tovar-Pescador, J. (2011). A high-resolution topographic correction method for clear-sky solar irradiance derived with a numerical weather prediction model. *Journal of Applied Meteorology and Climatology*, *50*(12), 2460–2472. https://doi.org/10.1175/2011JAMC2571.1

Saint-Martin, D., Geoffroy, O., Voldoire, A., Cattiaux, J., Brient, F., Chauvin, F., et al. (2021). Tracking changes in climate sensitivity in CNRM climate models. *Journal of Advances in Modeling Earth Systems*, *13*(6), e2020MS002190. https://doi.org/10.1029/2020MS002190

Schaaf, C., & Wang, Z. (2021). MODIS/Terra+Aqua BRDF/albedo albedo daily L3 global 0.05Deg CMG V061 [Dataset]. *NASA EOSDIS Land Processes DAAC*. https://doi.org/10.5067/MODIS/MCD43C3.061

Scoccimarro, E., Bellucci, A., & Peano, D. (2018). CMCC CMCC-CM2-VHR4 model output prepared for CMIP6 HighResMIP hist-1950 [Dataset]. *Earth System Grid Federation*. https://doi.org/10.22033/ESGF/CMIP6.3818

Scoccimarro, E., Peano, D., Gualdi, S., Bellucci, A., Lovato, T., Fogli, P. G., & Navarra, A. (2022). Extreme events representation in CMCC-CM2 standard and high-resolution general circulation models. *Geoscientific Model Development*, *15*(4), 1841–1854. https://doi.org/10.5194/gmd-15-1841-2022

Voldoire, A. (2019). CNRM-CERFACS CNRM-CM6-1-HR model output prepared for CMIP6 HighResMIP hist-1950 [Dataset]. *Earth System Grid Federation*. https://doi.org/10.22033/ESGF/CMIP6.4040

Volodin, E., Mortikov, E., Gritsun, A., Lykossov, V., Galin, V., Diansky, N., et al. (2019). INM INM-CM5-H model output prepared for CMIP6 HighResMIP hist-1950 [Dataset]. *Earth System Grid Federation*. https://doi.org/10.22033/ESGF/CMIP6.14050

Volodin, E., Mortikov, E., Kostrykin, S., Galin, V., Lykossov, V., Gritsun, A., et al. (2017). Simulation of the present-day climate with the climate model INMCM5. *Climate Dynamics*, *49*(11), 3715–3734. https://doi.org/10.1007/s00382-017-3539-7

von Rütte, F., Kahl, A., Rohrer, J., & Lehning, M. (2021). How forward-scattering snow and terrain change the alpine radiation balance with application to solar panels. *Journal of Geophysical Research: Atmospheres*, *126*(15), e2020JD034333. https://doi.org/10.1029/2020JD034333

von Storch, J.-S., Putrasahan, D., Lohmann, K., Gutjahr, O., Jungclaus, J., Bittner, M., et al. (2018). MPI-M MPI-ESM1.2-XR model output prepared for CMIP6 HighResMIP hist-1950 [Dataset]. *Earth System Grid Federation*. https://doi.org/10.22033/ESGF/CMIP6.10307

Wang, T., Yan, G., Mu, X., Jiao, Z., Chen, L., & Chu, Q. (2018). Toward operational shortwave radiation modeling and retrieval over rugged terrain. *Remote Sensing of Environment*, *205*, 419–433. https://doi.org/10.1016/j.rse.2017.11.006

Wang, Z., Wang, C., Yang, S., Lei, Y., Che, H., Zhang, X., & Wang, Q. (2022). Evaluation of surface solar radiation trends over China since the 1960s in the CMIP6 models and potential impact of aerosol emissions. *Atmospheric Research*, *268*, 105991. https://doi.org/10.1016/j.atmosres.2021.105991

Wild, M. (2008). Short-wave and long-wave surface radiation budgets in GCMs: A review based on the IPCC-AR4/CMIP3 models. *Tellus A: Dynamic Meteorology and Oceanography*, *60*(5), 932–945. https://doi.org/10.1111/j.1600-0870.2008.00342.x

Wild, M. (2017). Towards global estimates of the surface energy budget. *Current Climate Change Reports*, *3*(1), 87–97. https://doi.org/10.1007/s40641-017-0058-x

Wu, T., Yu, R., Lu, Y., Jie, W., Fang, Y., Zhang, J., et al. (2021). BCC-CSM2-HR: A high-resolution version of the Beijing climate center climate system model. *Geoscientific Model Development*, *14*(5), 2977–3006. https://doi.org/10.5194/gmd-14-2977-2021

Xu, J., Zhang, X., Zhang, W., Hou, N., Feng, C., Yang, S., et al. (2022). Assessment of surface downward longwave radiation in CMIP6 with comparison to observations and CMIP5. *Atmospheric Research*, *270*, 106056. https://doi.org/10.1016/j.atmosres.2022.106056

Yan, G., Tong, Y., Yan, K., Mu, X., Chu, Q., Zhou, Y., et al. (2018). Temporal extrapolation of daily downward shortwave radiation over cloud-free rugged terrains. Part 1: Analysis of topographic effects. *IEEE Transactions on Geoscience and Remote Sensing*, *56*(11), 6375–6394. https://doi.org/10.1109/TGRS.2018.2838143

Yang, X., Zhao, C., Zhou, L., Wang, Y., & Liu, X. (2016). Distinct impact of different types of aerosols on surface solar radiation in China. *Journal of Geophysical Research: Atmospheres*, *121*(11), 6459–6471. https://doi.org/10.1002/2016JD024938

Yi, B., Yang, P., Liu, Q., van Delst, P., Boukabara, S.-A., & Weng, F. (2016). Improvements on the ice cloud modeling capabilities of the community radiative transfer model. *Journal of Geophysical Research: Atmospheres*, *121*(22), 13577–13590. https://doi.org/10.1002/2016JD025207

Yu, L., Zhang, M., Wang, L., Lu, Y., & Li, J. (2021). Effects of aerosols and water vapour on spatial-temporal variations of the clear-sky surface solar radiation in China. *Atmospheric Research*, *248*, 105162. https://doi.org/10.1016/j.atmosres.2020.105162

Yu, Y. (2020). CAS FGOALS-f3-H model output prepared for CMIP6 HighResMIP hist-1950 [Dataset]. *Earth System Grid Federation*. https://doi.org/10.22033/ESGF/CMIP6.3316

Zakey, A. S., Solmon, F., & Giorgi, F. (2006). Implementation and testing of a desert dust module in a regional climate model. *Atmospheric Chemistry and Physics*, *6*(12), 4687–4704. https://doi.org/10.5194/acp-6-4687-2006

Zhang, X., Huang, A., Dai, Y., Li, W., Gu, C., Yuan, H., et al. (2022). Influences of 3D sub-grid terrain radiative effect on the performance of CoLM over Heihe river Basin, Tibetan plateau. *Journal of Advances in Modeling Earth Systems*, *14*(1), e2021MS002654. https://doi.org/10.1029/2021ms002654

Zhang, Y., Huang, A., & Zhu, X. (2006). Parameterization of the thermal impacts of sub-grid orography on numerical modeling of the surface energy budget over East Asia. *Theoretical and Applied Climatology*, *86*(1–4), 201–214. https://doi.org/10.1007/s00704-005-0209-1

Zhang, Y., Li, X., Cheng, G., Jin, H., Yang, D., Flerchinger, G., et al. (2018). Influences of topographic shadows on the thermal and hydrological processes in a cold region mountainous Watershed in Northwest China. *Journal of Advances in Modeling Earth Systems*, *10*(7), 1439–1457. https://doi.org/10.1029/2017ms001264

Zhao, M., Blanton, C., John, J. G., Radhakrishnan, A., Zadeh, N. T., McHugh, C., et al. (2018). NOAA-GFDL GFDL-CM4C192 model output prepared for CMIP6 HighResMIP hist-1950 [Dataset]. *Earth System Grid Federation*. https://doi.org/10.22033/ESGF/CMIP6.8567

Zhao, M., Golaz, J.-C., Held, I. M., Guo, H., Balaji, V., Benson, R., et al. (2018). The GFDL global atmosphere and land model AM4.0/LM4.0: 2. Model description, sensitivity studies, and tuning strategies. *Journal of Advances in Modeling Earth Systems*, *10*(3), 735–769. https://doi.org/10.1002/2017MS001209

Zheng, H., Chiew, F. H. S., Charles, S., & Podger, G. (2018). Future climate and runoff projections across South Asia from CMIP5 global climate models and hydrological modelling. *Journal of Hydrology: Regional Studies*, *18*, 92–109. https://doi.org/10.1016/j.ejrh.2018.06.004

Zheng, X., Tao, C., Zhang, C., Xie, S., Zhang, Y., Xi, B., & Dong, X. (2023). Assessment of CMIP5 and CMIP6 AMIP simulated clouds and surface shortwave radiation using ARM observations over different climate regions. *Journal of Climate*, *36*(24), 8475–8495. https://doi.org/10.1175/JCLI-D-23-0247.1

References From the Supporting Information

Kalogirou, S. A. (2014). Chapter 2 - environmental characteristics. In S. A. Kalogirou (Ed.), *Solar energy engineering* (2nd ed., pp. 51–123). Academic Press. https://doi.org/10.1016/B978-0-12-397270-5.00002-9

Kittler, R., & Darula, S. (2013). Determination of time and sun position system. *Solar Energy*, *93*, 72–79. https://doi.org/10.1016/j.solener.2013.03.021

Lawrence, D. M., Fisher, R. A., Koven, C. D., Oleson, K. W., Swenson, S. C., Bonan, G., et al. (2019). The Community Land Model version 5: Description of new features, benchmarking, and impact of forcing uncertainty. *Journal of Advances in Modeling Earth Systems*, *11*(12), 4245–4287. https://doi.org/10.1029/2018MS001583

Sharpnack, D. A., & Akin, G. (1969). An algorithm for computing slope and aspect from elevations. *Photogrammetric Engineering*, *35*(3), 247–248.

Skidmore, A. K. (1989). A comparison of techniques for calculating gradient and aspect from a gridded digital elevation model. *International Journal of Geographical Information Systems*, *3*(4), 323–334. https://doi.org/10.1080/02693798908941519

Vician, P., Palacka, M., Ďurčanský, P., & Jandačka, J. (2017). Determination of optimal position of solar trough collector. *Procedia Engineering*, *192*, 941–946. https://doi.org/10.1016/j.proeng.2017.06.162